Journal of the Brazilian Society of Mechanical Sciences and Engineering (2018) 40:297
https://doi.org/10.1007/s40430-018-1214-5

TECHNICAL PAPER

MCF-7 cancer cell apparent properties and viscoelastic characteristics measurement using AFM

Moharram Habibnejad Korayem[1] · Y. H. Sooha[1] · Z. Rastegar[1]

Received: 25 January 2018 / Accepted: 5 May 2018 / Published online: 16 May 2018
© The Brazilian Society of Mechanical Sciences and Engineering 2018

Abstract
Investigations on mechanical properties of biological cells especially cancer cells can considerably help recognizing various types of cancers. In this paper, we have concentrated on finding mechanical properties of breast cancer cell (MCF-7), elastic and viscoelastic, using atomic force microscopy. Initially, topography and apparent properties of the MCF-7 cell are studied, then the results are analyzed and compared with the literature to ensure the validity. After accurate diagnosis of MCF-7 cells, force–indentation curves for thirty-one cells, each in three different points, are obtained and the elasticity module of each point is calculated using Hertz and Dimitriadis theories. To ensure about the accuracy of experimental data, some statistical analysis is done to extract distribution functions for elasticity module of each theory. Due to the importance of adhesion force in the friction force, the purpose of this section is to determine adhesion changes in different points of the cell. In the next step, spring and viscosity force gradients and consequently stiffness and viscosity in different indentation depths are measured and finally appropriate creep function is extracted for viscoelastic behavior of MCF-7 using the Kelvin–Voigt model.

Keywords Cancer · Atomic force microscopy · Mechanical properties · Elastic properties · Viscoelastic properties · Elasticity module · Adhesion · Creep function

1 Introduction

Investigation of apparent properties and mechanical characteristics of MCF-7 cell develops the insight to better predicting its behavior and perhaps helps in more accurately recognizing different cancers. There are numerous devices utilized for measuring different properties of biological cells, one of which is an atomic force microscope (AFM) [1]. The main advantage of AFM compared to other methods is its applicability in obtaining other properties such as adhesion distribution, friction, elasticity module, viscoelastic characteristics besides, topography simultaneously [2]. AFM operates well in hard surfaces measurements but with softer surfaces such as cells or polymers, it faces several problems. Weisenhorn et al. obtained force–destination and force–indentation depth curves for elastomers, rubber and living biological cells in contact and concluded that the curves are parabolic. Then, elasticity module was obtained according to Hertz theory and the best force range in which the best clarity existed was represented [3].

Vinckier and Semenza measured elasticity module of biological materials using AFM. Using Hertz theory, they extracted the elasticity module and then they tried to measure this property of biological cells and soft matters using AFM [4]. Ikai et al. reviewed nano-mechanical methods using AFM. They obtained elasticity module using Hertz theory and indentation data [5].

Park and Lee measured mechanical properties in three different parts of a Muller cell. To do so, they put the AFM tip in touch with three different parts of the cell and obtained force–indentation depth curves [6].

Technical Editor: Estevam Barbosa Las Casas.

✉ Z. Rastegar
rastegar.afrooz@gmail.com

Moharram Habibnejad Korayem
hkorayem@iust.ac.ir

[1] Robotic Research Laboratory, Center of Excellence in Experimental Solid Mechanics and Dynamics, School of Mechanical Engineering, Iran University of Science and Technology, Tehran, Iran

Adhesion force behavior can be attributed to Van der Waals and capillary forces which exist between AFM tip and the surface. There is no capillary force in dry or vacuum environments, otherwise, due to environment humidity, there will be a capillary force which affects interaction between the tip and the surface. Magnitude of the capillary force depends on the tip–sample distance. The magnitude and sign of the force inserted by cantilever are related to its deviation and spring constant value [7].

Atomic force microscopy can be applied in recognition of geometry and mechanical properties of biological cells and their manipulation. Kasas et al. [8] studied mechanical properties—such as elasticity module, poison's ratio, and adhesion—of biological cells such as virus, bacteria, yeast, herbal cells and some mammalian cells by AFM. Li et al. calculated mechanical properties of red blood cell and three different types of cancer cells using AFM. Force–displacement curves and they showed that the elasticity module of healthy red blood cell as well as its diameter is less than three types of cancer cells [9].

Lee et al. calculated breast cancer cells properties using force–displacement curves obtained by AFM. Estimated shapes of these group particles were spherical and elliptical. Results showed that elasticity module for breast cancer cells is less than healthy ones [10]. Faria et al. tried imaging and recognition of three different types of prostate cancer cells properties. Cancer cells were cultivated in different days to have a more accurate investigation and the results of force–displacement experimental curve were explained by Hertz spherical elastic theory to calculate the properties [11]. Hui and Bany represented a contact model for viscoelastic spheres. Their model was a developed version of the JKR model. Their numerical simulation and previous experimental results were compatible. Still determining material energy level by this theory was hard and an alternative method should specify adhesion properties [12].

Cartagena and Raman investigated local viscoelastic properties of living cells using dynamic and quasi-static models based on AFM. Using AFM quasi-static force–indentation depth curves is the usual method for extracting elastic properties. In this work, the force gradient and losses on fibroblast cells in buffer solutions were reconstructed using Lorentz force excited cantilevers. Finally, stiffness and viscosity were locally measured and their difference—difference between the spring force and viscosity property of material—was obtained [13].

Zhai and McKenna modeled the viscoelastic contact problem of Nano-sphere and polyester surface in indentation tests. Illustrating limitations of the analysis have just been done by one load–indentation curve, they represented that this method does not determine total range of polymer viscoelastic response. They also showed that accomplishing one successive test including multiple loading rates or indentation rates which cover two or more degrees develops viscoelastic properties to a great extent [14].

Mechanical coupling between cells is a complicated process important for different biological processes. Biochemical therapies effects on cell–cell adhesion and individual cell mechanics have been investigated by AFM. A tipless cantilever was used to connect the cells. Cell–cell adhesion parameters such as maximum separation force and work of adhesion were extracted from the force–displacement curves [15]. Puech et al. [16] measured adhesion properties of zebra fish single cells for different substrates and concluded the extracellular connections effects on intracellular signaling.

In this paper, theories of elasticity module, adhesion force and viscoelastic characteristics measurements are initially studied. In the next step, sample preparation method, cell topography, experimental method, results and finally analysis and verification of each property introduced in the theory section have been presented.

2 Methods

2.1 Biological cell elasticity module

To extract necessary equations in order to calculate the cell elasticity module, force–indentation depth equations of contact model should be rewritten in terms of the elasticity module. Two bodies in contact are spheres with radii of R_1 and R_2. Effective radius between two particles would be defined as:

$$\frac{1}{\tilde{R}} = \frac{1}{R_1} + \frac{1}{R_2} \tag{1}$$

If the elasticity modules of two particles are E_1 and E_2, then the effective elasticity module will be shown as below:

$$\frac{1}{E^*} = \frac{\left(1 - v_1^2\right)}{E_1} + \frac{\left(1 - v_2^2\right)}{E_2} \tag{2}$$

where v is the poison's ratio. If the elasticity modules of two particles are E_1 and E_2, the effective elasticity module for circular geometry will be as follows [17]:

$$E^* = \frac{F}{\delta_{\text{Hertz}}^{1.5}\tilde{R}} \tag{3}$$

Finally, by having AFM tip data and cell poison's ratio, cell elasticity module can be calculated using Eq. (2).

There is a problem in using Hertz contact model since it does not consider sample's thickness and adhesion to the substrate. Dimitriadis et al. proposed an equation for

obtaining the elasticity module of the thin layers of soft matters utilizing AFM. In the case of indentation of the body 1 by the body 2, the elasticity module of the body 1 can be obtained by Eq. 4 [18]:

$$E_1 = \left(\frac{4\sqrt{R_2}}{3F(1-v_1^2)}\delta^{1.5}\left[1-\frac{2\alpha}{\pi}\chi+\frac{4\alpha^2}{\pi^2}\chi^2 - \frac{8}{\pi^3}\left(\alpha^3+\frac{4\pi^2}{15}\beta\right)\chi^3+\frac{16\alpha}{\pi^4}\left(\alpha^3+\frac{3\pi^2}{5}\beta\right)\chi^4\right]\right)^{-1} \tag{4}$$

In which $\chi = \sqrt{R_2\delta}/h$. h is the sample's thickness. α and β coefficients are dependent on adhesion of sample to substrate. For an adhesive sample (bonded):

$$\alpha = -0.347\frac{3-2v_2}{1-v_2} \tag{5}$$

$$\beta = 0.056\frac{5-2v_2}{1-v_2} \tag{6}$$

and for a non-adhesive sample:

$$\alpha = -\frac{1.2876-1.4678v_2+1.3442v_2^2}{1-v_2} \tag{7}$$

$$\beta = \frac{0.6387-1.0277v_2+1.5164v_2^2}{1-v_2} \tag{8}$$

Poison's ratio is usually considered about 0.5 for biological cells.

2.2 Adhesion force between cell and tip

In AFM device, the tip–sample interaction is used to measure surface adhesion force. Adhesion force magnitude between particles equals the force needed to separate them. In AFM, a sharp tip connected to the cantilever sweeps the sample surface. Engaged forces between tip and sample surface lead to deflection or deviation of cantilever and during sweeping, a detector measures the cantilever deflection. Finally, by converting deflection to force unit, engaged forces between tip and surface can be calculated.

Reliable results of adhesion force obtained through AFM cantilever bending need precise calibration of spring constant [19]. As mentioned before, obtained piezo position-bending curve is basically applied voltage to piezo in terms of cantilever position and it should be converted to adhesion force–destination curve. To convert piezo voltage to the adhesion force, calculating the voltage–destination curve slope in repulsive force region would be required [20]. Assuming that in repulsive forces region the sample will have no plastic deformation; piezo voltage conversion factor n can be converted to adhesion force as following.

$$m \times n = k\left(\left[\frac{\mathrm{mV}}{\mathrm{nm}}\right] \times \left[\frac{\mathrm{nN}}{\mathrm{mV}}\right] = \left[\frac{\mathrm{nN}}{\mathrm{nm}}\right]\right) \tag{9}$$

where k is cantilever spring constant which can be found in manufacturer catalog. In the case of inaccessibility, this magnitude should be extracted experimentally. Unfortunately, it is very complicated and no standard method has been represented already. There are different methods for estimating cantilever spring constant such as added mass, thermal noise, cantilever geometry based on theoretical methods, material properties and reference cantilever. Reference cantilever advantages are its cantilever force constant direct measurement in vacuum or air capability and its destructiveness. In this method, the bending of the cantilever with unknown spring constant k_{test} in compression to a cantilever with spring constant of k_{ref} and known elastic properties is used. If reference cantilever bending magnitude at the fixed end is δ_{tot} and at the free end is δ_{test}, then k_{test} can be obtained as follows [19]:

$$k_{\mathrm{test}} = k_{\mathrm{ref}}\frac{\delta_{\mathrm{tot}}-\delta_{\mathrm{test}}}{\delta_{\mathrm{test}}\cdot\cos\alpha} \tag{10}$$

where α is the angle between two cantilevers. To collide and have precise approaching to free end of a cantilever, its bending should be measured and assessed regularly (Fig. 1).

2.3 Viscoelastic characteristics of biological cell

Conventionally, elastic properties of biological cells are extracted using AFM force–indentation depth quasi-static curves. Obtaining viscoelastic properties can increase precision in cell mechanics.

Assuming that resultant frequency from cantilever Lorentz force is near the first frequency response, the equation of motion of single degree of freedom governing the tip $q(t)$ when oscillates far from the particle surface will be [13]:

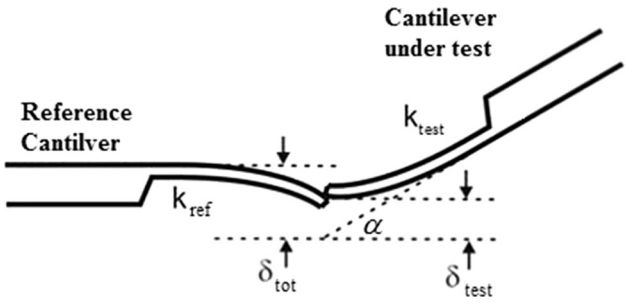

Fig. 1 Bending of the cantilever with unknown spring constant in different distances from the free end of cantilever

$$\frac{\ddot{q}}{\omega_{\text{far}}^2}+\frac{1}{\omega_{\text{far}}Q_{\text{far}}}\dot{q}+q=\frac{F_{\text{mag}}\ \sin(\omega_{\text{dr}}t)}{k_{\text{cant}}} \tag{11}$$

where ω_{far} is the cantilever resonance frequency (rad/s), Q_{far} is the quality factor far from the surface, ω_{dr} is the cantilever driving frequency (rad/s), F_{mag} is the magnitude of the magnetic excitation force, k_{cant} is calibrated cantilever spring constant and $\dot{q}$ is the tip velocity.

Solving the steady-state vibration response equation $q(t)=A_1\sin(\omega_{\text{dr}}t-\phi_1)$, it is shown that when ω_{dr} is tuned to the peak amplitude of the resonance curve far from the surface; we have [13]:

$$\omega_{\text{dr}}/\omega_{\text{far}}=\sqrt{1-\frac{1}{2Q_{\text{far}}^2}},\quad A_{1\text{far}}=\frac{F_{\text{mag}}}{k_{\text{cant}}}\frac{Q_{\text{far}}}{\sqrt{1-\frac{1}{4Q_{\text{far}}^2}}},\quad tg(\phi_{1\text{far}})=\sqrt{4Q_{\text{far}}^2-2} \tag{12}$$

where $A_{1\text{far}}$ is the oscillation amplitude and $\phi_{1\text{far}}$ is the phase lag far from the sample surface. When the drive is tuned at the resonance peak amplitude far from the sample, we should have [13]

$$F_{\text{mag}}=\frac{k_{\text{cant}}A_{1\text{far}}}{Q_{\text{far}}}\sqrt{1-\frac{1}{4Q_{\text{far}}^2}} \tag{13}$$

When the cantilever is approaching the sample, it interacts with soft cell surface so the motion equation would be:

$$\frac{\ddot{q}}{\omega_{\text{near}}^2}+\frac{1}{\omega_{\text{near}}Q_{\text{near}}}\dot{q}+q=\frac{F_{\text{mag}}\ \sin(\omega_{\text{dr}}t)+F_{\text{tp}}(Z+q,\dot{q})}{k_{\text{cant}}} \tag{14}$$

where F_{tp} is the tip–sample interaction force, Z is the distance between tip and particle with rigid cantilever assumption and ω_{near} is the cantilever resonance frequency near the sample. The cantilever motion while interacting with the sample is dominated by zeroth and first harmonics, which results in the following tip motion [13]:

$$q(t)=A_0+A_1\sin(\omega_{\text{dr}}t-\phi_1) \tag{15}$$

To convert these two harmonics, observables into local viscoelastic properties, we first interpret tip indentation into sample as follows [13]:

$$\delta(t)=Z+q=Z+A_0+A_1\sin(\omega_{\text{dr}}t-\phi_1) \tag{16}$$

During the living cells imaging, oscillation amplitude of tip A_1 is much smaller compared to indentation A_0; so $\delta_0=Z+A_0$. In fact, this part of indentation depth can be related to quasi-static force in elasticity module measurement. This means that indentation depth has been composed of two parts, quasi-static indentation δ_0 and dynamic indentation $\delta_{\text{dynamic}}=A_1\sin(\omega_{\text{dr}}t-\phi_1)$, $\delta=\delta_0+\delta_{\text{dynamic}}$. Interaction forces are defined as follows:

$$F_{\text{tp}}=F_{\text{tp}}^{\text{semi-static}}(\delta_0)+F_{\text{tp}}^{\text{dynamic}}(\delta-\delta_0) \tag{17}$$

The part of force related to zeroth harmonic, $F_{\text{tp}}^{\text{semi-static}}$, is a function of δ_0 and similarly interaction force related to the first harmonic or dynamic indentation, $F_{\text{tp}}^{\text{dynamic}}$, is a function of $\delta_{\text{dynamic}}=\delta-\delta_0$. Dynamic force itself is composed of two parts:

$$F_{\text{tp}}^{\text{dynamic}}=F_{\text{tp}}^{\text{s}}+F_{\text{tp}}^{\text{d}} \tag{18}$$

where F_{tp}^{s} is related to sample springiness and F_{tp}^{d} belongs to cell viscosity:

$$F_{\text{tp}}^{\text{s}}=k_{\text{sample}}^{\text{dynamic}}\left(\delta_{\text{dynamic}}\right),\quad F_{\text{tp}}^{\text{d}}=c_{\text{sample}}^{\text{dynamic}}\left(\dot{\delta}_{\text{dynamic}}\right) \tag{19}$$

where $k_{\text{sample}}^{\text{dynamic}}$ and $c_{\text{sample}}^{\text{dynamic}}$ are force interpretation of Kelvin–Voigt element parameters. For soft cantilevers resonance frequencies and Q factors near the sample (ω_{near} and Q_{near}) are different with measured magnitudes far from surface (ω_{far} and Q_{far}), due to hydrodynamic coupling between the cantilever and sample. Consequently, oscillation amplitude and phase lag near the surface differ from their magnitude far from the sample. The quantities near and far from the sample are related by [13]:

$$1-\left(\frac{\omega_{\text{dr}}}{\omega_{\text{near}}}\right)^2=\frac{A_{1\text{far}}\sqrt{1-\frac{1}{4Q_{\text{far}}^2}}}{A_{1\text{near}}Q_{\text{far}}}\cos(\phi_{1\text{near}}),\quad \frac{\omega_{\text{dr}}}{Q_{\text{near}}\omega_{\text{near}}}=\frac{A_{1\text{far}}\sqrt{1-\frac{1}{4Q_{\text{far}}^2}}}{A_{1\text{near}}Q_{\text{far}}}\sin(\phi_{1\text{near}}) \tag{20}$$

Finally, substituting (16) in (17) force parameters of Kelvin–Voigt will be:

$$k_{\text{sample}}^{\text{dynamic}}=\left(\frac{k_{\text{cant}}A_{1\text{far}}}{Q_{\text{far}}A_1}\cos(\phi_1)-\frac{k_{\text{cant}}A_{1\text{far}}}{Q_{\text{far}}A_{1\text{near}}}\cos(\phi_{1\text{near}})\right)\times\sqrt{1-\frac{1}{4Q_{\text{far}}^2}}$$
$$c_{\text{sample}}^{\text{dynamic}}=\left(\frac{k_{\text{cant}}A_{1\text{far}}}{Q_{\text{far}}A_1}\sin(\phi_1)-\frac{k_{\text{cant}}A_{1\text{far}}}{Q_{\text{far}}A_{1\text{near}}}\sin(\phi_{1\text{near}})\right)\times\sqrt{1-\frac{1}{4Q_{\text{far}}^2}} \tag{21}$$

Forces and displacements are equivalents of stresses and strains; thereby, stress parameters of Kelvin–Voigt can be obtained for force parameters. E_{sample} is the stress equivalent of $k_{\text{sample}}^{\text{dynamic}}$ and the stress equivalent of $c_{\text{sample}}^{\text{dynamic}}$ will be the viscosity coefficient η_{sample}. So, finding stresses and strains equivalent to dynamic interaction forces are important here upon which stress parameters of Kelvin–Voigt will be extracted.

As mentioned before, indentation depth and tip–sample interaction force are composed of two parts. The first part is related to quasi-static force and the second one is related to first harmonic and dynamic force. That part of force and indentation depth which belongs to first harmonic is important here. Stress and strain are defined as follows:

$$\varepsilon_{\text{dynamic}} = \frac{\delta_{\text{dynamic}}}{R_s - \delta_{\text{dynamic}}}, \quad \sigma_{\text{dynamic}} = \frac{F_{\text{tp}}^{\text{dynamic}}}{\pi a_{\text{dynamic}}^2} \tag{22}$$

where R_s is the sample radius and a_{dynamic} is the contact surface radius. Indentation causes indentation depth and contact radius, which can be related by Eq. (23) according to Hertz viscoelastic theory, developed in previous sections:

$$\delta = \frac{a^2}{\tilde{R}} \tag{23}$$

where $\tilde{R}$ is the effective radius defined as above. Since $\delta = \delta_0 + \delta_{\text{dynamic}}$, the contact radius can be divided into two parts too, $a^2 = a_0^2 + a_{\text{dynamic}}^2$. According to continuum mechanics for Kelvin–Voigt model, the relations between stress and strain in model branches, spring and viscosity branches, and total applied stress and strain will be:

$$\varepsilon_{\text{dynamic}} = \varepsilon_d = \varepsilon_s, \quad \sigma_{\text{dynamic}} = \sigma_d + \sigma_s \tag{24}$$

where ε_s and ε_d are related to springiness and viscosity, respectively, σ_s and σ_d are related to stresses of springiness and viscosity. Strain–stress relations for springiness branch and viscosity branch are $\sigma_s = E_{\text{sample}}\varepsilon_s$ and $\sigma_d = \eta_{\text{sample}}\dot{\varepsilon}_d$, respectively.

Since strain in two branches is equal, it can be concluded that contact radius due to each stress in branches is equal; so, if a_{dynamic}, a_s and a_d are, respectively, contact radius of dynamic indentation, springiness force and viscosity force; this equation will be established as $a_{\text{dynamic}} = a_s = a_d$. Finally, the equation for obtaining Kelvin–Voigt stress parameters will be:

$$\begin{aligned} E_{\text{sample}} &= \frac{k_{\text{sample}}^{\text{dynamic}}}{\pi\tilde{R}}\left(\frac{R_s - \delta_{\text{dynamic}}}{\delta_{\text{dynamic}}}\right), \\ \eta_{\text{sample}} &= \frac{c_{\text{sample}}^{\text{dynamic}}}{\pi\tilde{R}}\left(\frac{R_s - \delta_{\text{dynamic}}}{\delta_{\text{dynamic}}}\right)^2. \end{aligned} \tag{25}$$

3 Results

3.1 Sample preparation

MCF-7 breast cancer cells were prepared in SID breast cancer institute. The cells were cultivated in DMEM biological environment 2 days before the test. During the cultivation process, cultivation environment was kept in an incubator at 37 °C in a 5% CO_2 atmosphere to ensure their growth. Then, three thousand cells were separated and diluted in a volume of 2 ml of PBS along with 4% FBS. With use of a dropper precise volume of the solution was separated, in which an estimated number of 15–30 cells were existed. The droplet was put on a mica surface and was washed two times with PBS solution along with 4% FBS in 10 min to ensure minimum contamination. A special cap was put on a sample to prevent dusting. After 15 min, the sample was ready.

3.2 Imaging and cell topography

By locating the sample on its special position, the probe starts processing and identifying surface properties. Processed images are transferred to the computer connected to atomic force microscopy by the probe. Images are saved and recorded using the AFM software of the microscope manufacturer. The cell plane imaging position can be changed using atomic force microscopy utilities to complete a sweep of the surface by the probe. Figure 2 shows the images of three MCF-7 cells.

Geltmeier et al. [21] reported the MCF-7 cell volume in 3375–16,873 μm^3 range. Considering spherical geometry for these cells, their radius will be in the range of 9.3–15.9 μm. Taking a careful look at cells in Fig. 2, specified that the these three cells and other ones are in this range, so it can be said that recognized particles as MCF-7 are correctly identified.

3.3 Elasticity module

In this section, the experiment involves obtaining force–indentation curve for MCF-7 cancer cell. Force–indentation depth curves for cancer cell were obtained. Considering spherical geometry, the elasticity module can be calculated.

Force–indentation depth curves for three different points of eleven cells were obtained here. Then, elasticity moduli of each cell in three specified point were obtained using Hertz (Eq. 3) and Dimitriadis (Eq. 4) formulas. Figure 2 shows cell 1 and indentation points by AFM tip. Number I points are selected from top cells, number II from cell center and number III are selected from the cell edges in which cell thickness is decreasing. The goal was to obtain change rate of elasticity module in different points of the cell in order to extract elasticity module for every section using existing theory and assumption of known poison's ratio and also comparing the results to determine the difference between different points.

MCF-7 cells are considered spherical and with poison's ratio of 0.5. Also atomic force microscopy probe has the

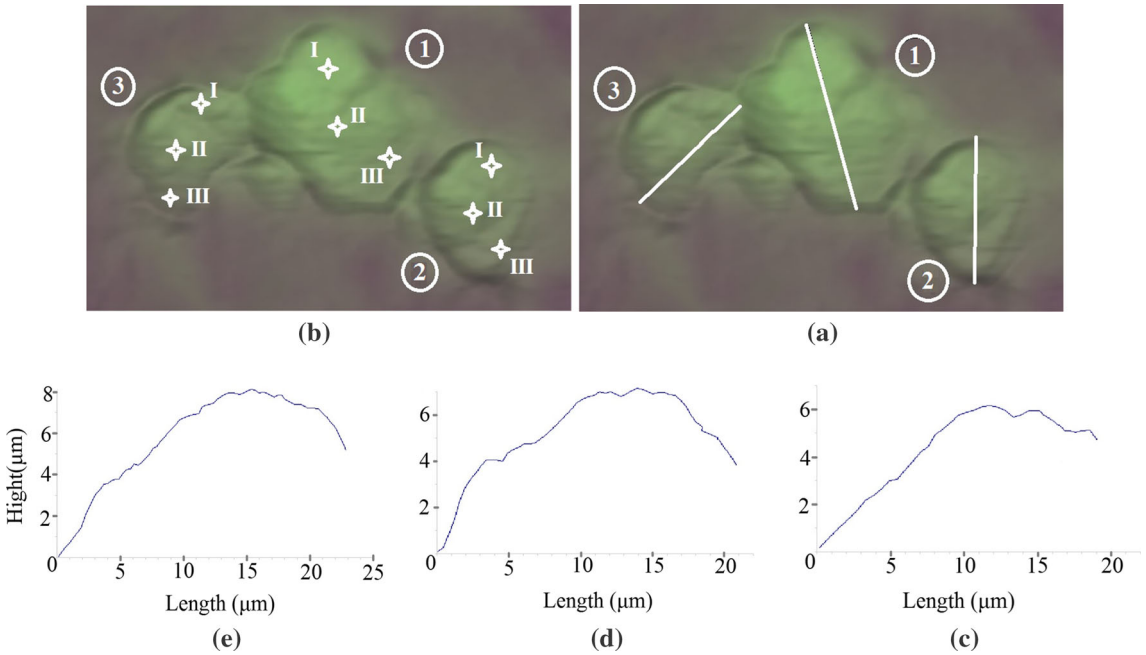

Fig. 2 Three indented MCF-7 cells. **a** Three MCF-7 cells for indentation, **b** indentation points in each cell, **c** number 3 cell surface profile, **d** number 2 cell surface profile, **e** number 1 cell surface profile

Table 1 Elasticity module (kPa) and adhesion force (μN)

	Cell #1				Average			
	Hight (μm)	Hertz (kPa)	Dimitriadis (kPa)	Adhesion (nN)	Hight (μm)	Hertz (kPa)	Dimitriadis (kPa)	Adhesion (nN)
Point I	5.64	1.51	1.15	137	5.24	1.58	1.06	142.3
Point II	8.11	1.31	0.98	58	7.71	1.37	0.9	83.3
Point III	4.93	1.83	1.35	161	4.49	1.81	1.39	207

spherical geometry and poison's ratio of 0.27. To obtain elasticity module in elastic case, Hertz (Eq. 3) and Dimitriadis (Eq. 4) formulas have been used. The results are summarized in Table 1.

According to Table 1, cell elasticity module at edges (number III points in Fig. 2) with less thickness is high and this property for the points with more thickness (number II points at each cell in Fig. 2) is low in comparison with other parts. Finally, the points of thickness between these two magnitudes (number I points at each cell in Fig. 2) have the elasticity module between these two points; depending on the thickness, their module will be near the point where the thickness is closer to the specified point. This result is analogous to the result obtained by Park and Lee in which their AFM probe was spherical. As shown in Fig. 2, the AFM tip was in touch with three different parts of the cell and force–indentation depth curves for every three parts were obtained by them. Considering AFM probe as a rigid sphere and cell as an elastic body and with assumption of known poison's ratio, they used Hertz theory to calculate elasticity module for all three parts. They concluded that the elasticity modules of cell beginning and end with less thickness are larger than other parts [1]. It can be explained by the fact that, with the less existence of intracellular liquid in the less thickness region, the membrane (which has similar behavior to solid materials) will play an important role and be more effective and consequently the elasticity module will be more in comparison with other regions (with larger thickness and more intracellular liquid. It can be said that since point III is thinner than other groups (points I and II), the obtained module for point III is more than two other points and point I has larger module in comparison with II.

In addition, obtained magnitudes in Table 1 should be noted. Geltmeier et al. [21] reported elasticity module of MCF-7 cell membrane to be about 1.125 kPa. Comparing obtained magnitudes for points II in each cell confirms that the obtained results are close to the reported magnitudes. In

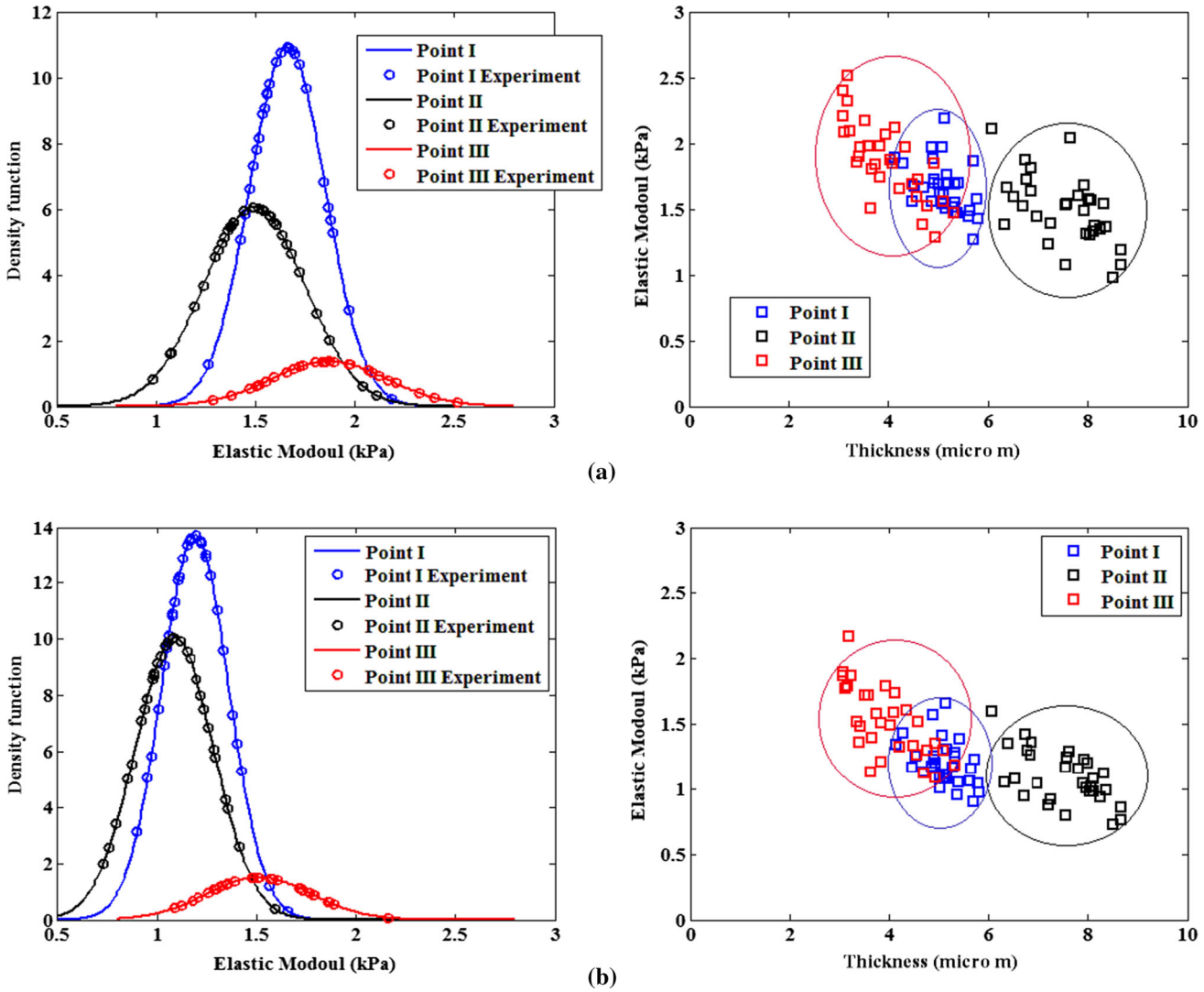

Fig. 3 (left) Distribution functions and (right) elasticity module-thickness diagrams for **a** Hertz and **b** Dimitrias theories

all three cells, the indentations have the similar patterns and, thus, the curves of cell II were represented and the full results were collected in Table 1 to avoid iteration. Also it can be said that the results can be confirmed by repeatability and following a similar pattern in three cells and their corresponding points.

Comparing elasticity modules' results of two different theories of Hertz and Dimitrias showed that measured magnitudes by Hertz theory for all three points and all cells and their averages are higher than Dimitras's results. This is because of the considering sample's thickness and its adhesion to the substrate in measurement of the elasticity modules by Dimitrias theory. To evaluate results statistically, extracted data were analyzed to obtain distribution functions (Fig. 3).

Figure 3 shows distribution functions and elasticity module-thickness diagrams of Hertz and Dimitrias theories. Elasticity module-thickness diagrams show that how thickness can affect elasticity module in these theories. Each circle is related to a special point of cells. The thickness of the cell at the indentation point is inversely related to elasticity module for both models. The points of the third group with the least thickness have the highest elasticity and vice versa. The normal function fitted for distribution function can help verifying experimental results. The area under the normal function in a special interval shows the possibility of occurrence. Since experimental data extracted from these tests are distributed over the curve with no or little dispersion, it can be concluded the average elasticity module obtained from these data is reliable. According to Geltmier et al., the MCF-10A cell's elasticity module is about 1.1 which is less than the magnitude obtained here for MCF-7 cell, so it can be said that

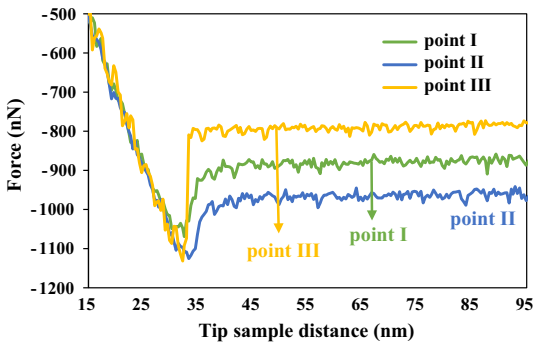

Fig. 4 Adhesion force–distance curve for cell #3 at different points

cancerous cells are stiffer than healthy cells based on comparison done between their elasticity module.

3.4 Adhesion

Atomic force microscopy can measure interaction forces between cantilever and its substrate using force spectroscopy. Piezo voltage–distance curves for different eleven cells were obtained. The points of adhesion force measurement are the points shown in Fig. 2. In this section, the goal was obtaining adhesion force changes rate in different points of cells to make a comparison to specify adhesion difference from point to point on a cell. The MCF-7 cell is considered spherical. During the tests, humidity was about 28% and the tip was approaching the sample surface and getting away at the speed of 261.4 nm/s. Table 1 shows the summarized results.

Since the process of tip approaching to sample and its returning in adhesion force-distance curves are the same, just the curves for third cell are shown in Fig. 4.

According to Table 1 and Fig. 4, it can be said that generally the maximum adhesion magnitudes are at points III, I and II, respectively. This result is similar to what obtained for elasticity module measurements. Result repeatability and following the same pattern confirm the results accuracy.

3.5 Viscoelastic characteristics (Kelvin–Voigt parameters)

Following assumptions should be met while doing tests and considered when during applying the theory:

1. The cantilever is moved directly with no oscillation or sample driving, so the cantilever has well-defined transfer function.
2. The tip is in constant contact with sample and oscillation amplitude in comparison with pure indentation of tip in the sample is small.
3. Special mode of cantilever oscillating far from the sample in comparison with the time compressing the sample is constant.
4. It should be identified that hydrodynamic correction on living cell in comparison with the fix is different.

Cantilever resonance frequency must be obtained after sample preparation and before the test. Since the resonance frequency slightly changes due to possible contaminations, this operation should be done before every test. Then, the probe driving frequency was chosen near the resonance curve peak and engaged in the cell. Cell topography was extracted at the same time with obtaining multi-harmonic data. Free amplitudes far from the sample $(A_{1\text{far}})$ are between 10 and 20 nm. Phase lag far from the sample tuned at $\phi_{1\text{far}}$ which, using the second term of Eq. (13), will be representative of low quality factor of $\phi_{\text{far}} = 5 - 13$. This change in amplitude and phase near to far from the cell in liquids which results from film hydrodynamic pressure between cantilever and cell surface is expected to be more but due to air environment of testing this effect is considerably reduced. Therefore, as expected, by approaching the tip to cell, oscillation amplitude and phase lag are slightly reduced (Table 2; Fig. 5).

These tests were repeated for 8 cells in three groups to ensure about results' repeatability. The first and second groups included 3 cells and the third one had 2 cells. Cells in each group were in similar size approximately, i.e., the average size of the first group was about 22.6, the second one about 19.3 and the third one 20.4 μm. Tests were done on different cells because repeating several tests on one cells could cause cell damage. Magnitudes in table are presented as average.

It can be observed that measured Kelvin–Voigt parameters are heavily dependent on indentation depth, as increased depth results in magnitude growth. Closer view implied that small drive frequency (to be more precise the quality factor far from the sample Q_{far} is lower) leads to larger Kelvin–Voigt parameters. This is the cause of high Kelvin–Voigt parameters for second cell despite smaller quality factor Q_{far} in comparison with other two cells. The quality factors of first and third cells are close but since the first cell has a lower quality factor Q_{far}, its Kelvin–Voigt parameters will be higher (Fig. 5). The same trend can be seen in the quality factor Q_{far} and measured phase difference ϕ_1 equation, i.e., the lower the quality factor far from the sample, the bigger the measured ϕ_1.

With closer look at Fig. 5 and Table 2, one could conclude that oscillation amplitude A_1 is not as effective as the quality factor. According to repeatability of the test results, it could be mentioned that the obtained results are correct and accurate. On the other hand, for verification, results can be compared to Cartagena and Raman work where

Table 2 Cantilever probe driving properties and frequency response

Group	ω_{dr} (Hz $\times 10^5$)	ω_{far} (Hz)	Q_{far}	A_{1far} (nm)	A_{1near} (nm)	ϕ_{1far} (°)	$\phi_{1\,near}$ (°)
#1	2.7837	278,993	10.626	17.32	17.26	87.30	86.85
#2	2.7645	278,960	5.283	14.66	14.64	95.45	93.96
#3	2.8757	278,995	12.860	11.21	11.18	87.77	86.43

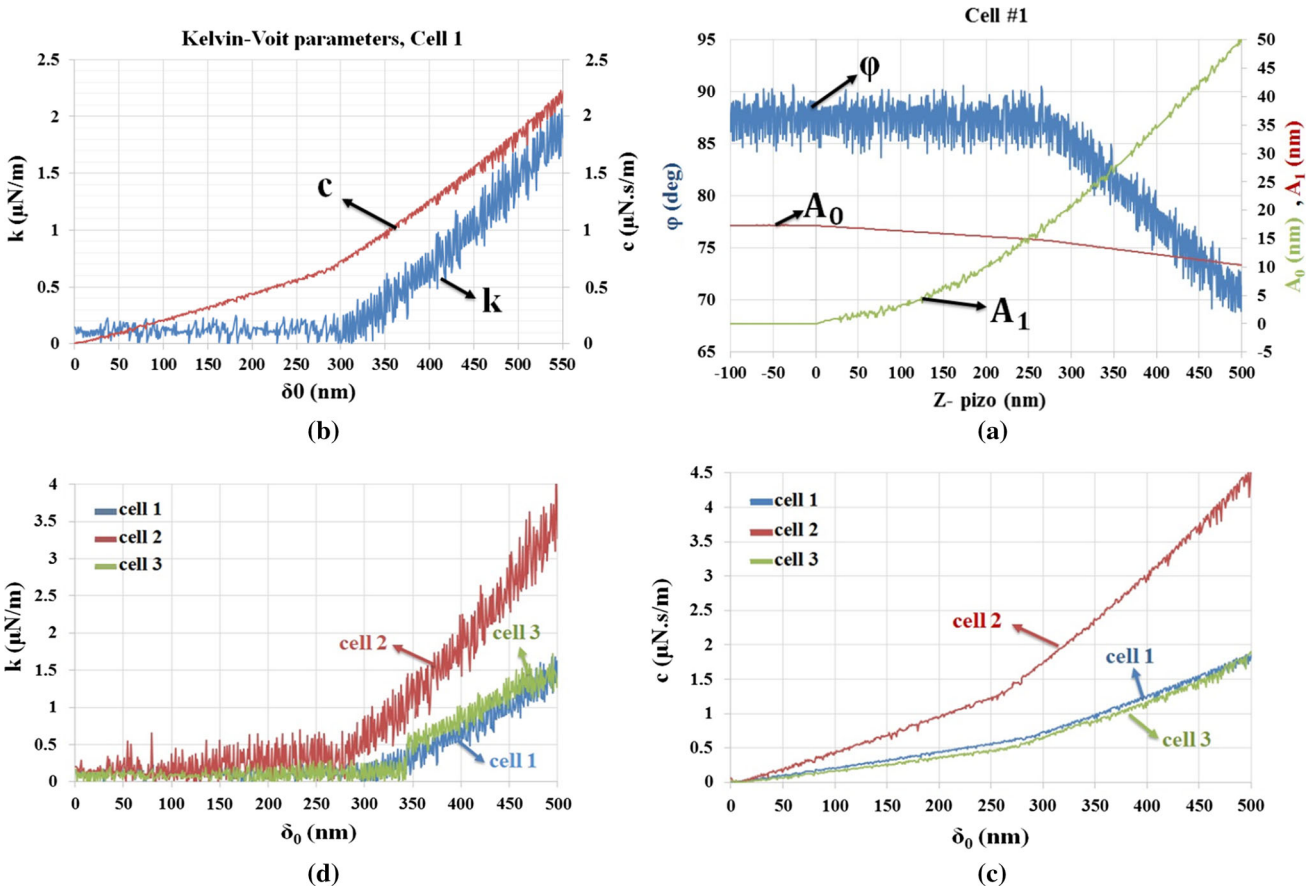

Fig. 5 Kelvin–Voigt force parameters comparison for first cell of first group. **a** Cell number 1 parameters of Eq. (15), **b** Kelvin–Voigt parameters obtained for first cell, **c** viscosity coefficient of three cells, **d** Spring constant of three cells

local viscoelastic characteristics of fibroblast cells have been extracted [13]. This comparison shows that obtained trend in measurable harmonic parameters and after that Kelvin–Voigt parameters for MCF-7 cell is similar to the fibroblast cell results of Cartagena and Raman.

In the case of viscoelastic models for cell, Kelvin–Voigt stress parameters used for more accurate representing the cell creep function are employed more than force parameters. After obtaining Kelvin–Voigt force parameters using Eq. (25), their stress equivalents can be calculated. Since the trend of the E_{sample} and η_{sample} are, respectively, similar to $k_{sample}^{dynamic}$ and $c_{sample}^{dynamic}$, it is unnecessary to go through details here; instead, after calculation of Kelvin–Voigt stress parameters in different indentation depths for each cell, the time constant $\left(\tau_{sample} = \eta_{sample}/E_{sample}\right)$ for each cell in different indentation depths will be calculated.

Then, using $C_{sample}(t) = \left(1/E_{sample}\right)\left(1 - e^{-t/\tau_{sample}}\right)$ (which obtained from continuum mechanics and explained in previous sections), creep function magnitudes for different depths were calculated. Since working with different magnitudes of E_{sample} and τ_{sample} for different depths is quite difficult, calculation of a single E_{sample} and τ_{sample} for each cell has been attempted. These magnitudes should be selected with how the theoretical creep function matches the calculated creep function magnitudes for that cell.

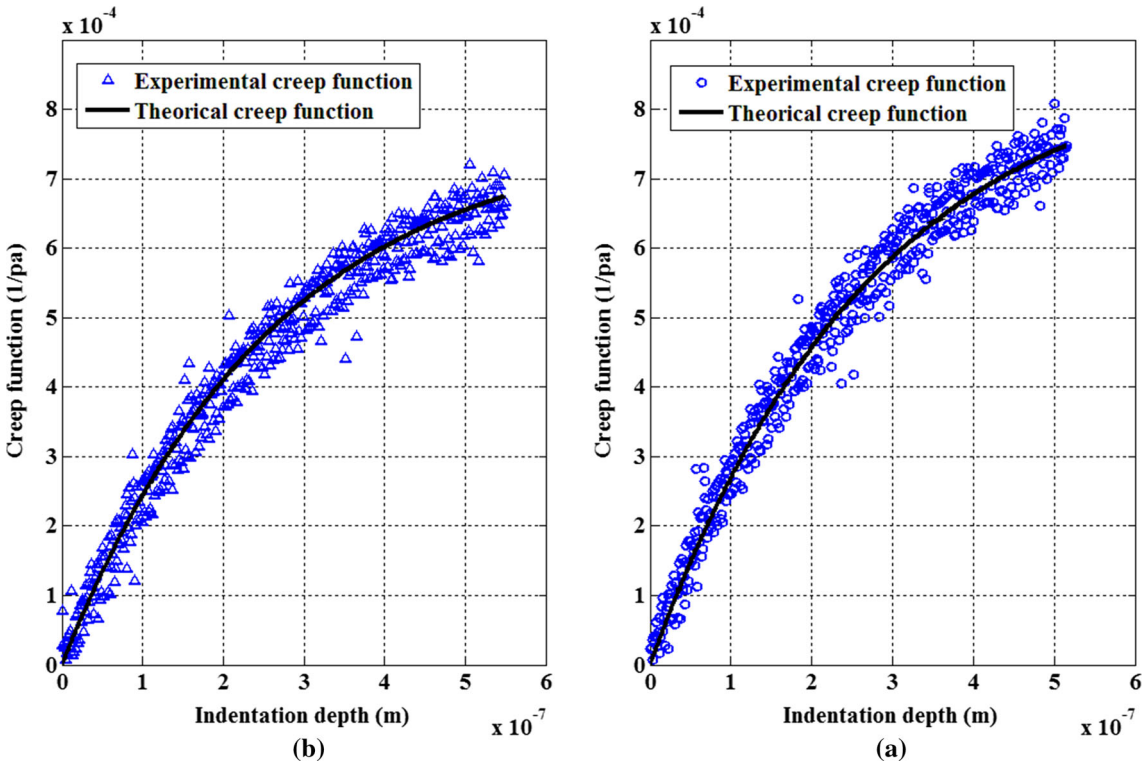

Fig. 6 Theoritical and experimental creep function for first and second cells from first group of cells. **a** Cell 1, **b** cell 2

Since for this creep function there are so many values for E_{sample} and τ_{sample}, it is more simple (explicit) to designate a more familiar magnitude to one of these parameters. In the second part of this report, elasticity module was measured in which the average elasticity module of MCF-7 cell for center points of cell represented about 1.377 kPa. So with assumption of this magnitude for cell, the time constant for each cell will be found. Figure 6 shows the experimental and theoretical creep function curve for first and second cells.

Average of time constants for first, second and third groups is 1.1, 1.05 and 1.25 s, respectively. Theoretical and experimental curves adaptation and repeatability of this magnitude confirm the results.

4 Conclusions and discussion

Identification of apparent properties and mechanical characteristics of biological cells especially cancer cells can increase the accuracy of their behavior prediction and these properties would considerably help in recognizing different types of cancers. Breast cancer is one of the most common cancers among women in which the cell is MCF-7. Atomic force microscopy is one of the most powerful tools in imaging and identifying the mechanical properties of unknown Nano-particles. In this paper, the topography was investigated and mechanical properties of MCF-7 cell such as elasticity module, adhesion force, and finally viscoelastic characteristics were extracted resulting in order to obtain the creep function. First, the topography and apparent properties of this cell were investigated and as a validation, the results were compared with the existing results of previous researches.

After accurate recognition of MCF-7 cells, the elasticity module was measured. In this step, the goal was obtaining the rate of elasticity moduli changes in different points of the cell. Force–indentation depth curves for three different points on eleven different cells were obtained. Then, using Hertz and Dimitriadis theories, the elasticity moduli of three different points on the surface of each cell were extracted. Number I points were selected on top of each cell, number II points in the center of cells and number III points at the edges in which the cell thickness is decreasing. Results showed that the maximum and minimum magnitudes of elasticity moduli are related to the points on the edges with smaller thickness (points III) and the points with larger thickness (points II), respectively. Elasticity module on the edges with smaller thickness (points III) is higher than other points and the points with larger thickness have lower module in comparison with other sites of

cells. Finally, points of thickness in between (points I) have elasticity module between these two magnitudes.

Adhesion force is one of the important factors in friction force development; thereby, the next test was adhesion obtaining between the cell and the tip. The largest magnitude of adhesion has been measured at points III, I and II, respectively. This result is the same as results obtained for the elasticity module. Eventually, by comparing the results of tests and predicted adhesion forces by contact theories, it has been demonstrated that the equations of contact theories were coincided with experimental results.

The usual method for extracting cell elastic properties is AFM force–indentation depth curves. Obtaining viscoelastic characteristics can increase the accuracy of cell mechanics. Viscoelastic characteristics were obtained from dynamic methods. In this paper, spring force and viscosity gradient and as a result stiffness and viscosity mechanical properties in different indentation depths were measured. Kelvin–Voigt model was used as a cell mechanics model. After obtaining force parameters of Kelvin–Voigt, stiffness and viscosity, their equivalents in stress–strain equations were obtained. With the calculation of stress parameters of Kelvin–Voigt at different indentation depths for each cell, time constants of each cell in different indentation depths were calculated. Then, creep function magnitude for different depths was calculated and it has been tried to extract a suitable and unique creep function for each cell which is compatible with the theoretical creep function. Finally, suitable creep function for MCF-7 cell was found which represented its viscoelastic behavior.

References

1. Rodriguez ML, McGarry PJ, Sniadecki NJ (2013) Review on cell mechanics: experimental and modeling approaches. Appl Mech Rev 65:e060801
2. Korayem MH, Khaksar H, Taheri M (2013) Modeling of contact theories for the manipulation of biological micro/nanoparticles in the form of circular crowned rollers based on the atomic force microscope. J Appl Phys 114:1–13
3. Weisenhorn AL, Khorsandi M, Kasas S, Gotzos V, Butt HJ (1993) Deformation and height anomaly of soft surfaces studied with an AFM. Nanotechnology 4:106–113
4. Vinckier A, Semenza G (1998) Measuring elasticity of biological materials by atomic force microscopy. FEBS Lett 430:12–16
5. Ikai A, Afrin R, Sekiguchi H, Okajima T, Alam MT (2003) Nanomechanical methods in biochemistry using atomic force microscopy. Curr Nanosci 4:181–193
6. Park S, Lee YJ (2013) Nano-mechanical compliance of Müller cells investigated by atomic force microscopy. Int J Biol Sci 9:546–554
7. Louey MD, Mulvaney P, Tewart PJS (2001) Characterization of adhesional properties of lactose carriers using atomic force microscopy. J Pharm Biomed Anal 25:559–567
8. Kasas S, Longo G, Dietler G (2013) Mechanical properties of biological specimens explored by atomic force microscopy. J Phys D Appl Phys 46:1–12
9. Li M, Liu L, Xi N, Wang Y, Dong Z, Xiao X, Zhang W (2012) Atomic force microscopy imaging and mechanical properties measurement of red blood cells and aggressive cancer cells. Sci China Life Sci 55:968–973
10. Li QS, Lee GYH, Ong CN, Lim CT (2008) AFM indentation study of breast cancer cells. Biochem Biophys Res Commun 374:609–613
11. Faria EC, Ma N, Gazi E, Gardner P, Brown M, Clarke NW, Snook RD (2008) Measurement of elastic properties of prostate cancer cells using AFM. Analyst 133:1498–1500
12. Hui CY, Baney JM (1998) Contact mechanics and adhesion of viscoelastic spheres. Langmuir 14:6570–6578
13. Cartagena A, Raman A (2014) Local viscoelastic properties of live cells investigated using dynamic and quasi static atomic force microscopy methods. Biophysical 106:1033–1043
14. Zhai M, McKenna GB (2014) Viscoelastic modeling of nanoindentation experiments: a multi-curve method. J Polym Sci Part 52:633–639
15. Siamantouras E, Hills E, Squires PE, Liu K (2014) Nano-mechanical investigation of soft biological cell adhesion using atomic force microscopy. Cell Mol Bioeng 8:22–31
16. Puech H, Taubenberger A, Ulrich F, Krieg M, Muller DJ, Heisenberg CP (2005) Measuring cell adhesion forces of primary gastrulating cells from zebra-fish using atomic force microscopy. J Cell Sci 118:4199–4206
17. Hertz H (1881) Über die Berührung fester elastischer Körper. Journal für die reine und angewandte Mathematik 92:156–171
18. Dimitriadis EK, Horkay F, Maresca J, Kachar B, Chadwick RS (2002) Determination of elastic moduli of thin layers of soft material using the atomic force microscope. Biophys J 82:2798–2810
19. Stegemann B, Backhaus H, Kloss H, Santner E (2007) Spherical AFM probes for adhesion force measurements on metal single crystals. Mod Res Educ Top Microsc 64:820–827
20. Çolak A (2013) Measuring adhesion forces between hydrophilic surfaces with atomic force microscopy using flat tips. University of Twente, Enschede. https://doi.org/10.3990/1.9789036516129
21. Geltmeier A, Rinner B, Bade D, Meditz K, Witt R, Bicker U, Bludszuweit Philipp C, Maier P (2015) Characterization of dynamic behavior of MCF7 and MCF10A cells in ultrasonic field using modal and harmonic analyses. PLoS ONE 10:e0134999